JUSTC

Review

http://justc.ustc.edu.cn

Received: September 24, 2021; Accepted: April 20, 2022

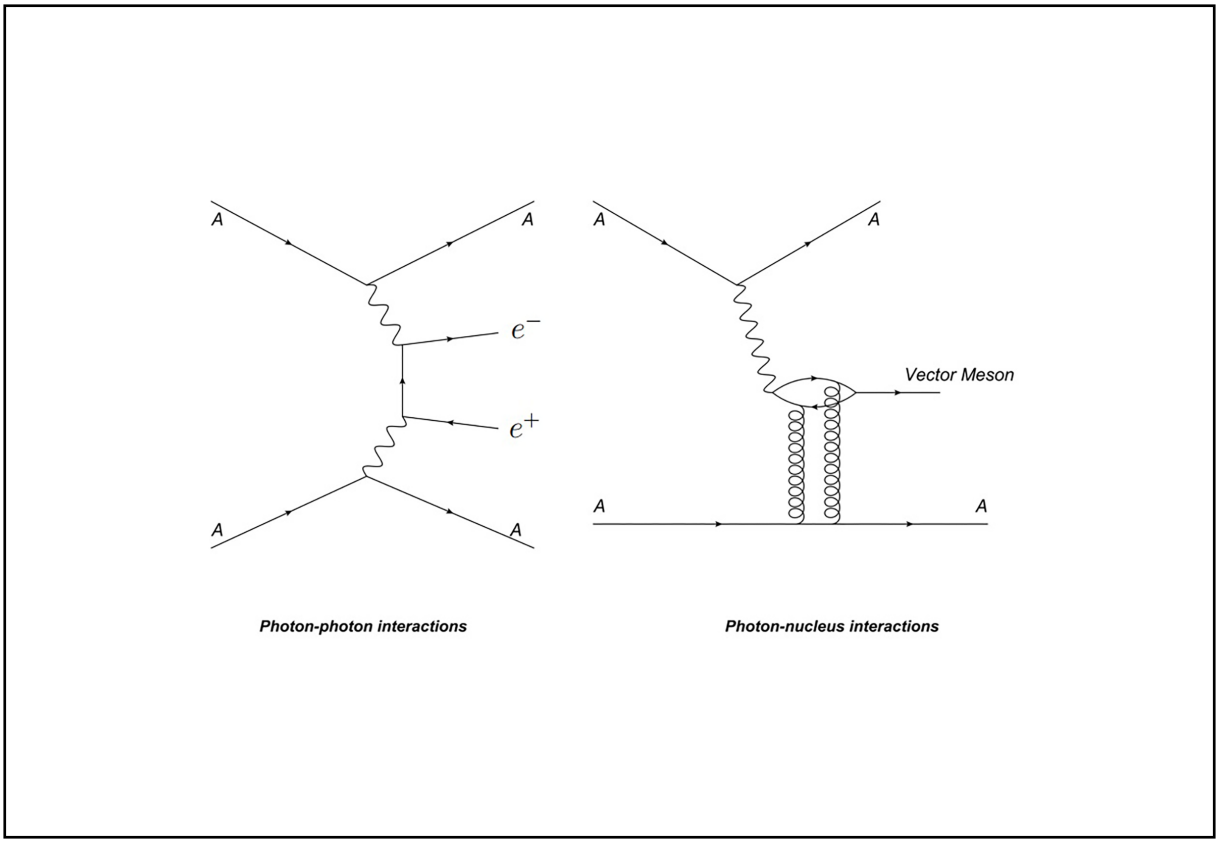
Coherent photoproduction processes in hadronic heavy-ion collisions

Jiaxuan Luo[1,2], Xin Wu[1,2], Jian Zhou[1,2], Wangmei Zha[1,2] ✉, and Zebo Tang[1,2]

[1]*State Key Laboratory of Particle Detection and Electronics, University of Science and Technology of China, Hefei 230026, China;*
[2]*Department of Modern Physics, University of Science and Technology of China, Hefei 230026, China*

✉Correspondence: Wangmei Zha, E-mail: first@ustc.edu.cn
© 2022 The Author(s). This is an open access article under the CC BY-NC-ND 4.0 license (http://creativecommons.org/licenses/by-nc-nd/4.0/).

Graphical abstract



Photoproduction processes in relativistic heavy-ion collisions.

Public summary

- We review and summarize the recent experimental and theoretical progresses on the coherent photoproduction of J/ψ and dilepton in hadronic heavy-ion collisions.
- According to the calculations of the phenomenological model, the excesses of J/ψ and dilepton production at very low transverse momentum in hadronic heavy-ion collisions may result from the photoproduction processes.
- J/ψ and dilepton, originating from the coherent photoproduction process in relativistic heavy-ion collisions, may serve as new novel probes to study the evolution of quark-gluon plasma and to determine electromagnetic properties of QGP.

Citation: Luo J X, Wu X, Zhou J, et al. Coherent photoproduction processes in hadronic heavy-ion collisions. *JUSTC*, **2022**, 52(6): 3. DOI: 10.52396/JUSTC-2021-0210

JUSTC

Review

http://justc.ustc.edu.cn

Received: September 24, 2021; Accepted: April 20, 2022

Coherent photoproduction processes in hadronic heavy-ion collisions

Jiaxuan Luo[1,2], Xin Wu[1,2], Jian Zhou[1,2], Wangmei Zha[1,2] ✉, and Zebo Tang[1,2]

[1]*State Key Laboratory of Particle Detection and Electronics, University of Science and Technology of China, Hefei 230026, China;*
[2]*Department of Modern Physics, University of Science and Technology of China, Hefei 230026, China*

✉Correspondence: Wangmei Zha, E-mail: first@ustc.edu.cn
© 2022 The Author(s). This is an open access article under the CC BY-NC-ND 4.0 license (http://creativecommons.org/licenses/by-nc-nd/4.0/).

Cite This: *JUSTC*, **2022**, 52(6): 3 (15pp)

Read Online

Abstract: Recently, significant abnormal enhancements in J/ψ and dilepton production have been observed in peripheral heavy-ion collisions at very low transverse momentum by the STAR, ALICE and ATLAS Collaborations. The observed excesses cannot be explained by hadronic production combined with the cold and hot medium effects, though it can be well described by coherent photoproduction calculations with nuclear overlap. These experimental and theoretical results provide evidence of coherent photoproduction in hadronic heavy-ion collisions, which suggest novel probes for detecting the properties of quark-gluon plasma (QGP). In this work, we review recent experimental and theoretical progress regarding coherent photoproduction in hadronic heavy-ion collisions.

Keywords: hadronic heavy-ion collision; quark-gluon plasma; coherent photoproduction; J/ψ; dilepton

CLC number: O571.6 **Document code:** A

1 Introduction

The major physical goal of the Relativistic Heavy Ion Collider (RHIC) at Brookhaven National Laboratory and the Large Hadron Collider (LHC) at CERN is to search for a new form of matter, quark-gluon plasma[1] (QGP), which is predicted by lattice quantum chromodynamics (QCD). J/ψ and dileptons are considered important probes for studying the properties of the quark-gluon plasma.

Because of the color screening effect in the deconfined hot medium[2], J/ψ production should be suppressed in heavy-ion collisions, which has been proposed as a direct signal of quark-gluon plasma formation. After decades of experimental and theoretical investigations, it has been realized that the regeneration effect of charm quarks in the QGP[3] and the cold nuclear matter (CNM) effect[4] can significantly affect the production of J/ψ in heavy-ion collisions. Currently, models incorporating color screening, regeneration, and CNM effects can reasonably describe J/ψ suppression in heavy-ion collisions at super proton synchrotron, RHIC, and LHC energies[5].

In relativistic heavy-ion collisions, dileptons have been proposed as penetrating QGP probes because they are immune to the strong interactions and are produced during the entire evolution of the medium. The main sources of dileptons include hadronic cocktail, QGP thermal radiation, and in-medium broadening of the ρ mass spectrum[6,7]; the hadronic cocktail consists of lepton pair contributions from known hadronic sources (e.g., the direct or Dalitz decay of π^0, η, η', ω, Φ, J/ψ, ψ', $c\bar{c}$, $b\bar{b}$, and the Drell-Yan process).

In addition to hadronic production, J/ψ and dileptons can also be generated by ultra-strong electromagnetic fields accompanied with the colliding nuclei. In relativistic heavy-ion collisions, the electromagnetic fields are compressed into the transverse plane (perpendicular to the direction of motion of the heavy ions) due to the Lorentz contraction. The electric and magnetic fields are mutually perpendicular, share the same absolute value, and very similar to the electromagnetic fields of photons. Thus, the transverse electromagnetic fields can be viewed as an equivalent swarm of photons[8]. In 1924, Fermi first proposed the idea of equivalent photon approximation[9] (EPA); later, Williams and Weizsäcker [10] independently extended Fermi's idea into the so-called Weizsäcker-Williams method. In the view of the equivalent photon approximation, J/ψ can be produced via coherent photon–nucleus interactions in relativistic heavy-ion collisions, and dilepton can be produced by coherent photon–photon interactions; that is, virtual photons emitted by one nucleus can fluctuate into $q\bar{q}$ pairs, scatter off the other nucleus, and emerge as vector mesons; or interact with photons emitted by the other nucleus to produce dileptons. This coherent photoproduction process has been widely studied in ultra-peripheral collisions (UPCs)[11]. In these collisions, the impact parameter is more than twice as large as the nuclear radius, ensuring that the two colliding nuclei have no overlap region and no hadronic interaction occurs. In ultra-peripheral collisions, the products of the coherent photoproduction process contain only two complete nuclei and vector mesons or dileptons with extremely low transverse momentum. From a conventional viewpoint, coherent photoproduction processes are only expected in UPCs to meet the coherence requirement. In hadronic heavy-ion collisions, the two colliding nuclei are broken; here, the coherent requirement cannot be satisfied and the coherent photoproduction processes should be forbidden.

DOI: 10.52396/JUSTC-2021-0210
JUSTC, **2022**, 52(6): 3

Recently, the ALICE[12], STAR[13,14], and ATLAS[15] Collaborations have observed significant excesses of J/ψ and dilepton production at very low transverse momentum in peripheral hadronic heavy-ion collisions. The excess J/ψ cannot be explained by the color screening, regeneration, or CNM effects, and the excess dileptons cannot be described by the hadronic cocktail, QGP thermal radiation and in-medium broadening of the ρ mass spectrum. These excesses indicate that, alongside hadronic production, other production mechanisms for J/ψ and dilepton are present in hadronic collisions. Furthermore, the excesses exhibit features of coherent photoproduction, which indicates the existence of coherent photoproduction in hadronic heavy-ion collisions. This significantly challenges our understanding of coherent photoproduction in heavy-ion collisions.

In this review, we summarize recent experimental and theoretical progress in the coherent photoproduction of J/ψ and dilepton in hadronic heavy-ion collisions. In the second section we discuss the research progress regarding J/ψ production via coherent photon-nucleus interactions. The research progress regarding dilepton production via coherent photon-photon interactions is summarized in the third section. The final section presents the discussion and future prospects.

2 J/ψ production from coherent photon–nucleus interactions in hadronic heavy-ion collisions

J/ψ production via the coherent photonuclear interaction $\gamma + A \rightarrow J/\psi + A$ can be viewed as a photon-Pomeron fusion process in relativistic heavy-ion collisions; this offers an opportunity to directly determine the gluon distribution in the nucleons and nuclei[16]. This additional production process for J/ψ in hadronic heavy-ion collisions may provide a novel probe for QGP.

2.1 Measurements of the ALICE Collaboration

The ALICE Collaboration [17,18] reported the measurements of J/ψ production at very low transverse momentum (p_T < 0.3 GeV/c) via their $\mu^+\mu^-$ decay channel in peripheral Pb + Pb collisions at $\sqrt{s_{\rm NN}}$ = 2.76 TeV. In this measurement, ~ 17×10^6 dimuon minimum bias ($\mu\mu$MB) events were collected via triggering on opposite sign (OS) tracks detected in the muon spectrometer triggering system[12]. A silicon pixel detector (SPD), scintillator arrays (V0), and zero degree calorimeters (ZDCs) were used in this analysis. The SPD provides the coordinates of the primary interaction vertex, whereas the V0 and ZDCs provide timing information, that reduces the background induced by the beam and electromagnetic processes.

Fig. 1 shows the transverse momentum distributions of raw OS dimuons without combinatorial background subtraction for the invariant mass range 2.8 GeV/c^2 < $m_{\mu^+\mu^-}$ < 3.4 GeV/c^2 in 70%–90% Pb + Pb collisions at $\sqrt{s_{\rm NN}}$ = 2.76 TeV. The red line denotes the transverse momentum distribution predicted by the STARLIGHT Monte Carlo generator[19] convoluted with the response function of the muon spectrometer. A remarkable excess of dimuons was observed at very low p_T in this centrality class.

To quantitatively describe the excess J/ψ production in hadronic A + A collisions with respect to that in p + p collisions, the nuclear modification factor $R_{\rm AA}$ was used; it is defined as follows:

$$R_{\rm AA} = \frac{1}{< T_{\rm AA} >} \frac{{\rm d}^2N_{\rm AA}/{\rm d}p_T{\rm d}y}{{\rm d}^2\sigma_{\rm pp}/{\rm d}p_T{\rm d}y} \quad (1)$$

where ${\rm d}^2N_{\rm AA}/{\rm d}p_T{\rm d}y$ is the J/ψ yield in A+A collisions, ${\rm d}^2\sigma_{\rm pp}/{\rm d}p_T{\rm d}y$ is the J/ψ cross-section in p + p collisions, and $<T_{\rm AA}>$ is the average value of the nuclear thickness function. Fig. 2 shows the J/ψ nuclear modification factor as a function of $N_{\rm part}$ for three different transverse momentum intervals in Pb + Pb collisions at $\sqrt{s_{\rm NN}}$ = 2.76 TeV. The J/ψ $R_{\rm AA}$ (shown in Fig. 2) exhibits a significant increase in the p_T range of 0–0.3 GeV/c; this could not be described by any of the transport models[20, 21], because these transport models only consider hadronic production.

The p_T shape of the observed excess resembles that of J/ψ produced by coherent photon–nucleus interactions[22] in UPCs, one plausible explanation is that the excess at very low transverse momentum is attributed to coherent photoproduction in hadronic heavy-ion collisions. The average transverse momentum of the coherently photoproduced J/ψ was ~0.055

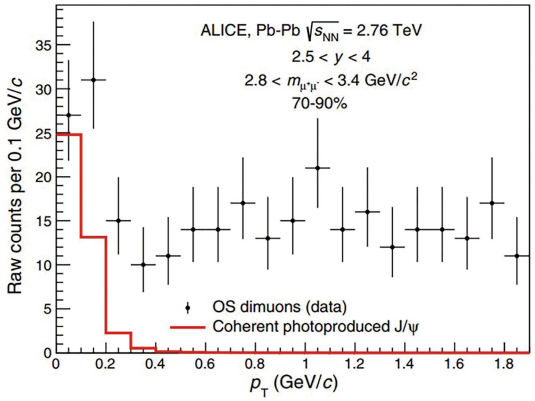


Fig. 1. Raw OS dimuon p_T distribution for invariant mass range 2.8 GeV/c^2 < $m_{\mu^+\mu^-}$ < 3.4 GeV/c^2 in 70%–90% Pb + Pb collisions at $\sqrt{s_{\rm NN}}$ = 2.76 TeV. Vertical error bars denote statistical uncertainties. Figure taken from Ref. [12].

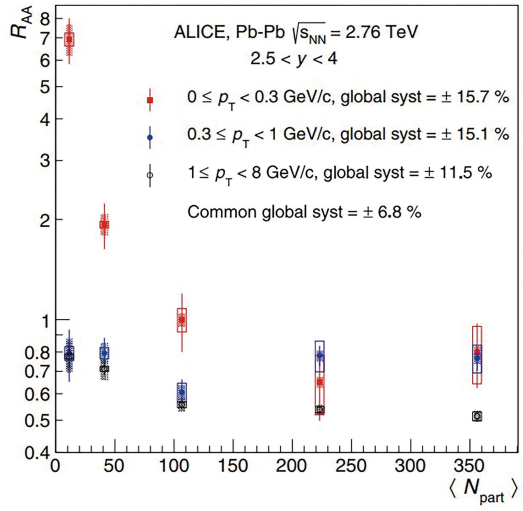


Fig. 2. J/ψ $R_{\rm AA}$ as a function of $N_{\rm part}$ for three p_T intervals in Pb + Pb collisions at $\sqrt{s_{\rm NN}}$= 2.76 TeV. Figure taken from Ref. [12].

DOI: 10.52396/JUSTC-2021-0210
JUSTC, **2022**, 52(6): 3

GeV/c. The detector effects can widen the reconstructed transverse momentum distribution; hence, 98% of the coherently photoproduced J/ψ are contained in the transverse momentum interval [0, 0.3] GeV/c [12].

Via an in-depth study of the photoproduction mechanism, Ref. [23] successfully explained the observed excesses using the Boltzmann transport model, which includes the photoproduction, initial hadronic production, regeneration, and decay of B hadrons. Figs. 3 and 4 show the J/ψ inclusive nuclear modification factor as a function of the number of participants ($N_{\rm part}$) for different production mechanisms in three different transverse momentum intervals, where the total production (color band) includes the contribution from the decay of the B hadrons. The nuclear modification factor $R_{\rm AA}$ in p_T < 0.3 GeV/c (Fig. 3) at $N_{\rm part}$ ⩽ 100 is much larger than that in p_T > 0.3 GeV/c (Fig. 4). Coherent photon–nucleus interactions are responsible for the excess of $R_{\rm AA}$ in the very low transverse momentum bin.

2.2 Measurements of the STAR Collaboration

The STAR Collaboration measured J/ψ production at very low transverse momentum using the Au + Au data collected during the 2010–2011 RHIC runs at $\sqrt{s_{\rm NN}}$ = 200 GeV and the U + U data collected in 2012 at $\sqrt{s_{\rm NN}}$ = 193 GeV [13]. The total number of events used in the Au + Au and U + U collisions were 720 million and 270 million, respectively. The collision centrality is determined by comparing the measured particle multiplicity with the Monte Carlo Glauber model simulation[24], and only data from 0–80% central collisions are accepted, to avoid the significant inefficiency of the vertex position detector in peripheral collisions. J/ψ can be reconstructed through their decay into electron-positron pairs, and the branch ratio of this decay channel is BR ($J/\psi \to e^+ + e^-$) = (5.97 ± 0.03)%[25]. The acceptance and efficiency correction procedure used is very similar to that in Ref. [5]; furthermore, to meet the coherent production requirement[26], the J/ψ at very low transverse momentum is set with a transverse polarization. The correction factors were ~20% lower than those obtained without polarization assumption.

Fig. 5 shows the J/ψ invariant yields for Au + Au collisions at $\sqrt{s_{\rm NN}}$ = 200 GeV and U + U collisions at $\sqrt{s_{\rm NN}}$ = 193 GeV as a function of p_T for different centralities at midrapidity ($|y|$ < 1), as measured by the STAR Collaboration; here, the solid lines in the figure represent the fitting to data points in the range of p_T > 0.2 GeV/c, obtained using[27]

$$\frac{{\rm d}^2N}{2\pi p_T {\rm d}p_T {\rm d}y} = \frac{a}{(1+b^2p_T^2)^n} \tag{2}$$

where a, b, and n are free parameters. The dashed lines denote the extrapolated fits, which can well describe the data points in the range of p_T > 0.2 GeV/c but underestimate the yields in the range of p_T < 0.2 GeV/c for noncentral collisions (20%–80%).

Fig. 6 shows the J/ψ nuclear modification factor as a function of p_T in Au + Au and U + U collisions for different centrality classes; J/ψ suppression was observed in all centralities for p_T > 0.2 GeV/c. This is consistent with previous measurements[5], and can be described well by transport models[21,20] incorporating modifications from cold and hot medium effects. However, at very low transverse momentum (p_T < 0.2 GeV/c) and a significant enhancement of J/ψ, $R_{\rm AA}$ is observed in peri-

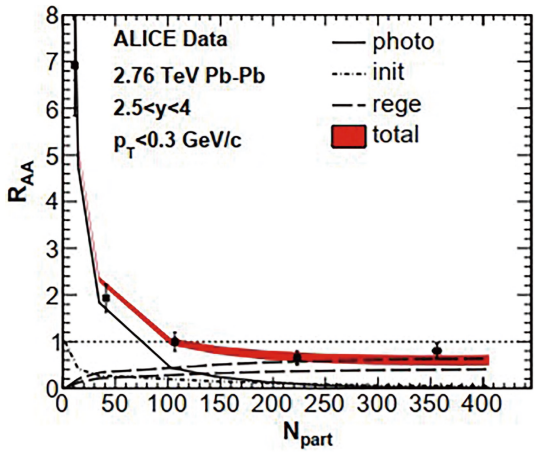


Fig. 3. J/ψ inclusive nuclear modification factor as a function of the number of participants $N_{\rm part}$ for p_T < 0.3 GeV/c in 2.76 TeV Pb + Pb collisions at forward rapidity 2.5 < y < 4. Figure taken from Ref. [23].

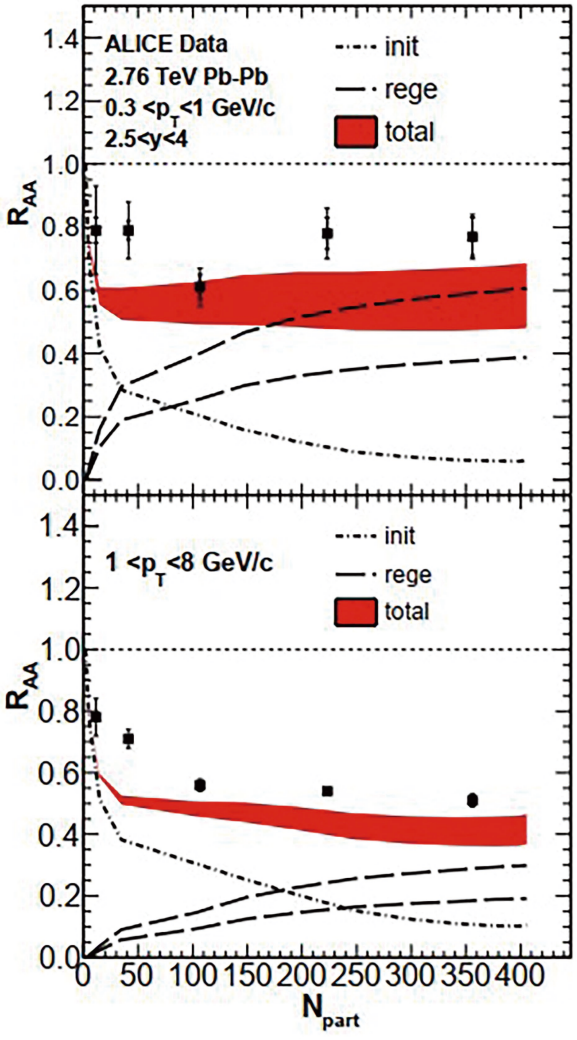


Fig. 4. J/ψ inclusive nuclear modification factor as a function of the number of participants $N_{\rm part}$ in 0.3 < p_T < 1 and 1 < p_T < 8 GeV/c in forward rapidity 2.5 < y < 4 at LHC 2.76 TeV Pb + Pb collisions. Figure taken from Ref. [23].

DOI: 10.52396/JUSTC-2021-0210
JUSTC, **2022**, 52(6): 3

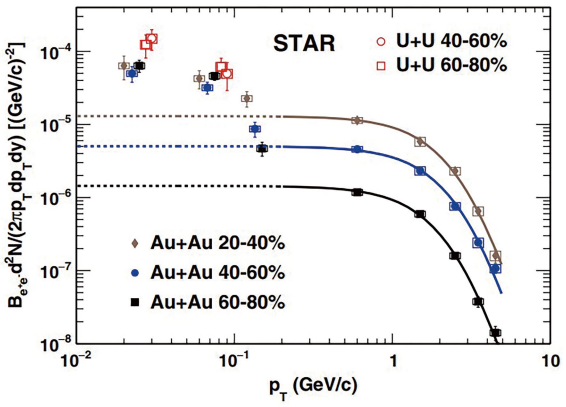


Fig. 5. J/ψ invariant yields for Au + Au collisions at $\sqrt{s_{\rm NN}}$ = 200 GeV and U + U collisions at $\sqrt{s_{\rm NN}}$ = 193 GeV as a function of p_T for different centralities. The error bars depict the statistical errors and the boxes denote the systematic uncertainties. Figure taken from Ref. [13].

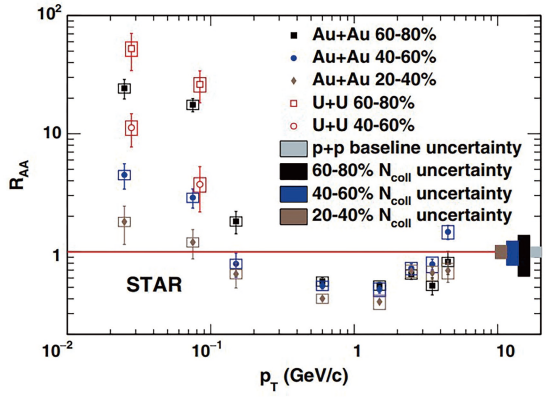


Fig. 6. J/ψ $R_{\rm AA}$ as a function p_T in Au + Au collisions at $\sqrt{s_{\rm NN}}$ = 200 GeV and U + U collisions at $\sqrt{s_{\rm NN}}$ = 193 GeV. Figure taken from Ref. [13].

pheral collisions (40%–80%) for both Au + Au and U + U collisions. In this p_T range, the color screening effect and CNM effect suppress J/ψ production, and the regeneration effect (which increases J/ψ production) is negligible[20]. The overall effect results in $R_{\rm AA} < 1$ for hadronic production; however, the $R_{\rm AA}$ shown in the figure well exceeds the theoretical value, which strongly suggests the existence of other production mechanisms for J/ψ.

To explore the source of the J/ψ enhancement, the STAR Collaboration further studied the dependence of J/ψ yield on collision centrality and compared it with the contribution from hadronic production. Fig. 7 shows the p_T-integrated J/ψ yields for $p_T < 0.1$ GeV/c with the expected hadronic contribution subtracted as a function of $N_{\rm part}$ for Au + Au and U + U collisions. As shown in that, at low transverse momentum, the hadronic contribution is not dominant in the measured centrality classes and increases dramatically toward central collisions; meanwhile, the measured excess shows no significant dependence on centrality within the uncertainties. Assuming that coherent photoproduction causes the excess at very low transverse momentum, because the yield of coherently photoproduced J/ψ is proportional to Z^2, the excess in U + U collisions should exceed that in Au + Au collisions, as shown in Fig. 7. However, within the limitations of the measurement precision, the observed difference was not significant (2.0σ)[13].

2.3 Phenomenological model calculation

In peripheral collisions, the impact parameter is less than twice the radius, and the colliding nuclei break apart. The photon–nucleus interaction cross-section was calculated by the equivalent photon approximation[28], quantum Glauber model[24], and vector meson dominance model[29]; the strong interactions in the overlap region were considered. To describe the contribution of hadronic interactions, the coherent photon–nucleus process was divided into two sub-processes: photon emission and coherent scattering.

For photon emission, photons are likely to be emitted before hadronic interactions occur; therefore, photon emission should be unaffected by hadronic interactions. However, the nucleons in the overlap region of the target nucleus should exhibit a reduced photon flux for the scattering process because the effective photon flux decreases toward the center of the emitter[28]. Hence, there are two limiting cases for photon emission: either the entire nucleus (nucleus) or only the spectator nucleons (spectator) act as the emitter. For coherent scattering, the spectator nucleons that are not affected by hadronic interactions can still act coherently; however, the participating nucleons that undergo violent hadronic interactions do not meet the coherent production requirement. Therefore, two limiting cases are considered for coherent scattering: either the entire nucleus (nucleus) or only spectator nucleons (spectator) act coherently. Finally, there are four different coupling scenarios for coherent J/ψ production: (i) nucleus (emitter) + nucleus (target), (ii) nucleus + spectator, (iii) spectator + nucleus, and (iv) spectator + spectator[28].

Fig. 7 also shows the model calculations of coherent photoproduction for Au + Au collisions in the above four coupling scenarios. The yields of coherently produced J/ψ can be modified by the color screening effect, which is not considered in the model. All four scenarios can describe the data well for the 60%–80% collision centrality class, which indicates the contribution of coherent photoproduction to the excess J/ψ at very low transverse momentum. However, in more central

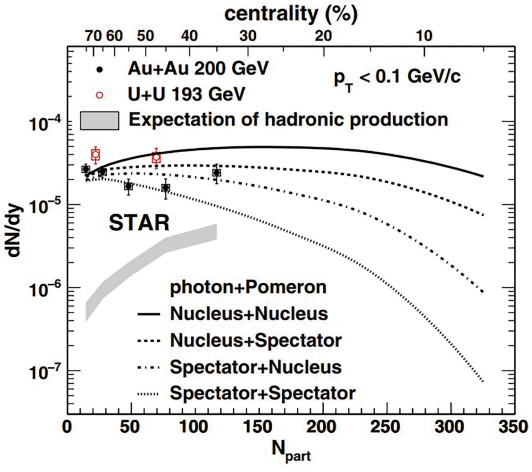


Fig. 7. The p_T-integrated J/ψ yields ($p_T < 0.1$ GeV/c) with expected hadronic contribution subtracted as a function of $N_{\rm part}$ for 30%–80% Au + Au collisions and 40%–80% U + U collisions. Lines denote the model calculations for coherent photoproduction in four coupling scenarios. Figure taken from Ref. [13].

DOI: 10.52396/JUSTC-2021-0210
JUSTC, **2022**, 52(6): 3

collisions, the nucleus + nucleus scenario significantly overestimates the data, suggesting a disruptive effect of coherent photoproduction by strong hadronic interactions in the overlap region[13]. Advanced models with color screening effects and more precise measurements in central collisions are required to study coherent production under different scenarios in the future.

The isobaric collision experiment was recently completed in 2018 at RHIC, and the STAR Collaboration collected three billion Ru + Ru ($^{96}_{44}$Ru) and Zr + Zr ($^{96}_{40}$Zr) collision events. According to the equivalent photon approximation, the J/ψ yield from the coherent photon–nucleus interaction is proportional to Z^2. Therefore, if the coherent photo–nucleus interactions cause the excess in Au + Au collisions at very low p_T, then the yield of coherently produced J/ψ in Ru + Ru collisions and Zr + Zr collisions should be much lower than in Au + Au collisions; meanwhile, the Ru and Zr nuclei have similar nuclear profiles but the number of protons Z differs, so the J/ψ yield from coherent photoproduction in Ru + Ru collisions should slightly exceed that in Zr + Zr collisions.

Fig. 8 depicts the coherent J/ψ yields as a function of $N_{\rm part}$ in Au + Au, Ru + Ru, and Zr + Zr collisions at $\sqrt{s_{\rm NN}}$ = 200 GeV at very low transverse momentum[30]. The yields first increased and then decreased with $N_{\rm part}$. The increase in J/ψ yield from peripheral to semi-peripheral collisions resulted from the larger photon flux attributable to the smaller impact parameter, and the later inversion of the trend originates from the disruptive effect of hadronic interactions in the overlap region. The production rate in Ru + Ru collisions was 1.2 times that in Zr + Zr collisions, and the production rate in Au + Au collisions was approximately four times that in Ru + Ru or Zr + Zr collisions, following the exact Z^2 scaling.

2.4 Double-slit experiment at Fermi scale

The double-slit experiment has become a classic thought experiment for expressing wave–particle complementarity. To date, such wave-particle duality has been studied in a broad range of entities, including electrons[31], neutrons[32], helium atoms[33], C_{60} fullerenes[34], and biomolecules[35]. In relativistic heavy-ion collisions, the transverse momentum of the coherently produced vector meson, J/ψ, is extremely low. When two ions collide, if the information describing which one of the two nuclei emits a virtual photon and which one acts as the target is missing, the vector meson originates simultaneously from both colliding nuclei and behaves as a wave[36]. The coherently photoproduced vector mesons provide a new double-slit scenario at Fermi scale in heavy-ion collisions, further demonstrating the complementarity principle.

Ref. [36] performed a Fourier transform on the amplitudes of two gold nuclei in coordinate space, to obtain the probability distribution of J/ψ in momentum space. The results for coherent J/ψ photoproduction in ultra-peripheral collisions are shown in Fig. 9, where Panels Figs. 9a–9c depict the amplitude distribution in the coordinate space and Panels Figs. 9d–9f indicate the probability distribution in the momentum space. Panels Figs. 9a and 9d assume that the two nuclei are point-like particles; typical Young's double-slit interference fringes can be observed. Panels Figs. 9b and 9e take the density profile of the nucleus into account and assume it to be subject to the Woods-Saxon distribution, expressed as

$$\rho_A(r) = \frac{\rho^0}{1+\exp[(r-R_{WS})/d)]} \tag{3}$$

where the parameter ρ^0 is the normalization factor, and the radius R_{WS} and skin depth d are based upon fits to the electron scattering data[37]. The profile of the slits means that typical diffraction rings can be observed in the momentum space. Panels Figs. 9c and 9f show the distributions as modified by

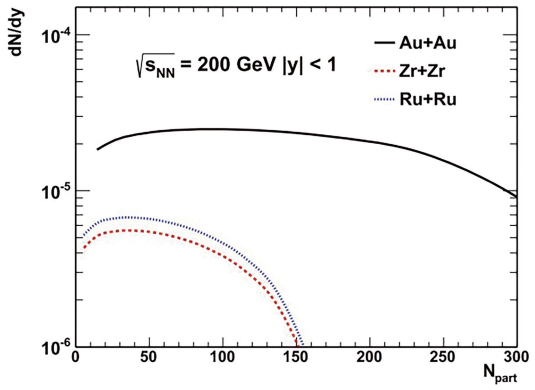


Fig. 8. Coherent J/ψ production yields as a function of $N_{\rm part}$ at $\sqrt{s_{\rm NN}}$ = 200 GeV in Au + Au, Ru + Ru, and Zr + Zr collisions. Figure taken from Ref. [30].

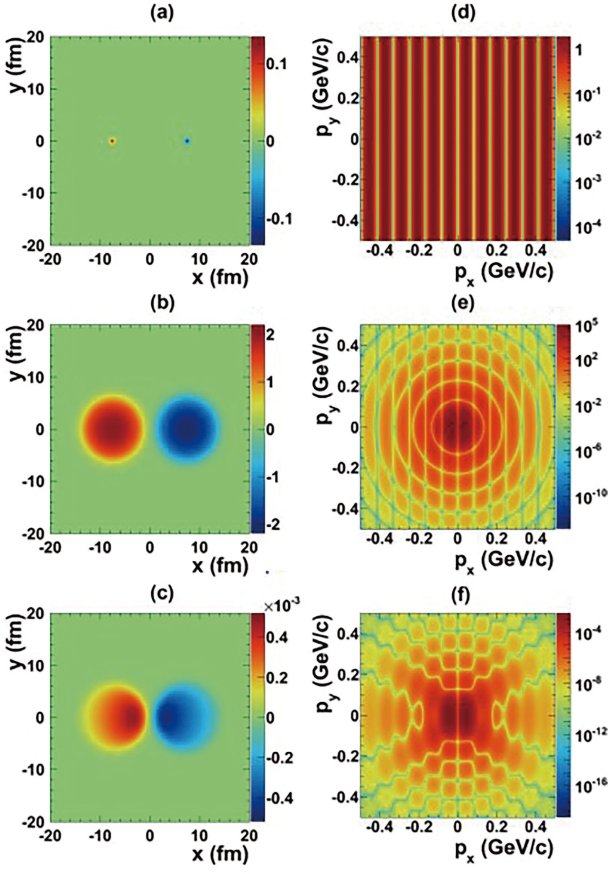


Fig. 9. Amplitude and momentum distribution patterns of coherent J/ψ photoproduction in different scenarios for b = 10 fm in Au + Au collisions at $\sqrt{s_{\rm NN}}$ = 200 GeV at midrapidity (y = 0). Figure taken from Ref. [36].

DOI: 10.52396/JUSTC-2021-0210
JUSTC, **2022**, 52(6): 3

the space photon flux, nuclear shadowing, and coherence length effect; these effects cause the slits to become asymmetric. As shown in the figure, the interference fringes become curved, and the diffraction does not show the typical symmetric rings.

However, in peripheral collisions, where the impact parameter is less than twice the radius, the disruptive effect from the overlap region must be considered. In the overlap region, the strong interactions between nucleons are short-range; thus, the which-way information can be obtained within the range of strong interactions, which means that the which-way problem is partially solved[36]. To simplify calculation, the assumption that the which-way information is only obtained in the initial overlap region is adopted, and the corresponding results are shown in Fig. 10, where Panels Figs. 10a and 10d show the impact parameter b = 13.0 fm, Panels Figs. 10b and 10e show b = 10.0 fm, and Panels Figs. 10c and 10f show b = 5.7 fm.

2.5 Photoproduction and hadroproduction

J/ψ has different production mechanisms in different transverse momentum bins[23]. As shown in Fig. 11, the coherently photoproduced J/ψ is mainly distributed in the range of p_T< 0.1 GeV/c. Beyond this p_T bin, the hadroproduction (which mainly includes the initial production, regeneration, and decay of B hadrons) becomes dominant. The J/ψ from regeneration is mainly distributed below 3–5 GeV/c, and the J/ψ produced by the initial production and decay of the B hadrons becomes important at higher transverse momentum bins.

Fig. 12 shows the charmonium photoproduction and initial hadroproduction (both without modifications from cold and hot medium effects) as a function of the number of participants $N_{\rm part}$ at the forward rapidity 2.5 < y < 4 at very low transverse momentum (p_T < 0.3 GeV/c) in Pb + Pb collisions at $\sqrt{s_{\rm NN}}$ = 2.76 TeV, which can help us to clearly understand the relationship between the two production mechanisms. The electromagnetic fields produced by the two nuclei first increase and then decrease with $N_{\rm part}$; thus, the photoproduction reaches its maximum value in semi-central collisions. At $N_{\rm part}$> 200 (b < 7 fm), the hadroproduction is approximately five times larger than the photoproduction[23].

The interaction between the quark and its antiquark of quarkonium is very violent, which makes it difficult for the quarkonium to dissociate. However, QGP contains copious free quarks, antiquarks, and gluons, which can interact with the quark or antiquark of quarkonium, resulting in dissociation of the quarkonium (i.e., the color screening effect)[38]. Because of this effect, the interaction between the c and $\bar{c}$ of J/ψ in QGP becomes weak; subsequently, J/ψ suffers from dissociation and the yield is suppressed.

The J/ψ from hadroproduction is only distributed in the overlap region of the two nuclei, where QGP is produced; meanwhile, the J/ψ from coherent photoproduction is distributed over the entire nuclear surface. Therefore, the QGP suppression of photoproduction is always weaker than that of

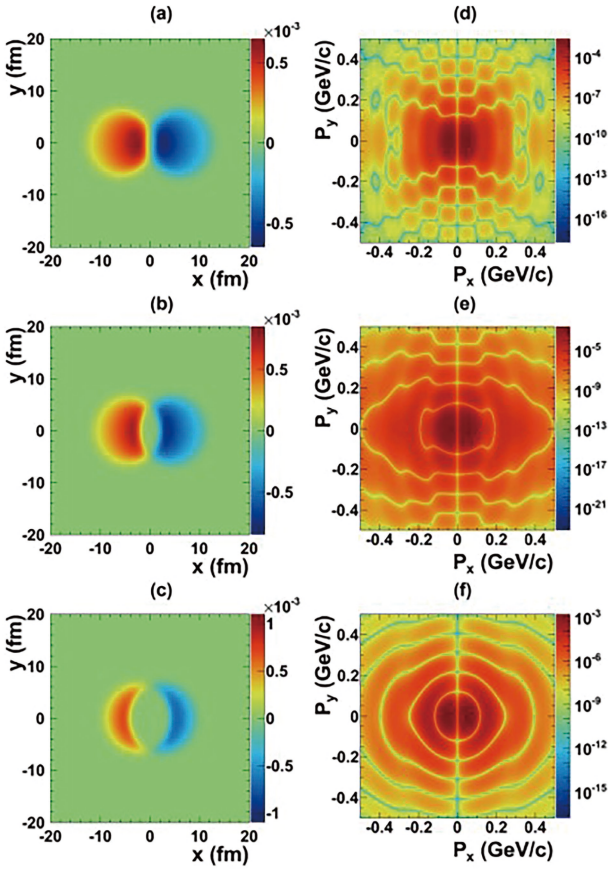


Fig. 10. Amplitude and momentum distribution patterns of coherent J/ψ photoproduction at midrapidity (y = 0) in Au + Au collisions at $\sqrt{s_{\rm NN}}$ = 200 GeV with a disruptive effect from the overlap region for different impact parameters. Figure taken from Ref. [36].

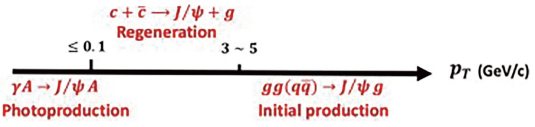


Fig. 11. Schematic diagram for different charmonium production mechanisms at different transverse momentum regions in semi-central nucleus–nucleus collisions in the presence of both QGP and strong transverse electromagnetic fields. Photoproduction, regeneration, and initial production dominate the J/ψ final yields in extremely low p_T, low and middle p_T, and high p_T regions, respectively. Figure taken from Ref. [23].

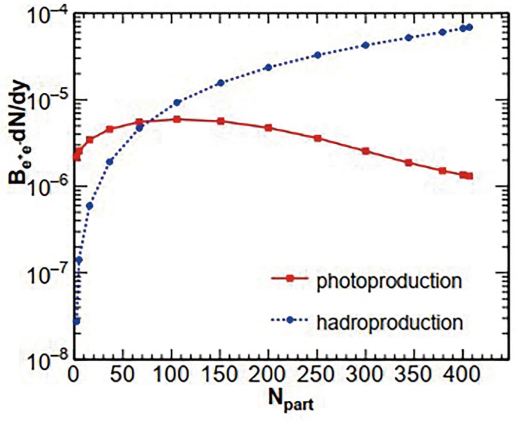


Fig. 12. Charmonium hadroproduction and photoproduction as a function of the number of participants $N_{\rm part}$ at forward rapidity 2.5 < y < 4 in $\sqrt{s_{\rm NN}}$ = 2.76 TeV Pb + Pb collisions in the extremely low transverse momentum region p_T < 0.3 GeV/c. $B_{e^+e^-}$ is the branch ratio of $J/\psi \to e^+e^-$. Figure taken from Ref. [23].

DOI: 10.52396/JUSTC-2021-0210
JUSTC, 2022, 52(6): 3

hadroproduction. When $N_{\rm part}$ is between 100 and 150, the initial temperature of the QGP is approximately $2T_c$, and 20%–40% of the photoproduced J/ψ undergoes dissociation via the color screening effect and parton inelastic collisions, where T_c is the critical temperature of the deconfined phase transition[39].

Fig. 13 shows the dependence of different charmonium production mechanisms upon the transverse momentum in $\sqrt{s_{\rm NN}}$ = 2.76 TeV Pb + Pb collisions with impact parameter b = 10.2 fm and forward rapidity $2.5 < y < 4$; here, the two dashed lines indicate a 20% difference, attributable to the large uncertainties of the production cross-section measured by experiments. In the $p_T < 1$ GeV/c region, the nuclear modification factor $R_{\rm AA}$ of photoproduction is significantly enhanced, whereas the distribution of hadroproduction is relatively flat, and the regeneration falls to zero at $p_T \sim 3$ GeV/c. In higher transverse momentum regions, charmonium primarily includes the initial production from parton hard scattering.

2.6 Summary

Conventionally, because of the coherence requirement, coherent J/ψ photoproduction has only been studied and predicted in ultra-peripheral heavy-ion collisions. However, the ALICE and STAR Collaborations have recently observed a significant enhancement of J/ψ yields at extremely low transverse momentum in hadronic heavy-ion collisions, and the observed excesses exhibit the features of coherent photoproduction, which provides evidence of coherent vector meson photoproduction in hadronic collisions. The phenomenological model calculations with coherent photoproduction can describe the excesses observed at STAR and ALICE very well, and they suggest that disruption from the violent hadronic interactions occurs between nucleons in the overlap region during coherent photoproduction. To further investigate the coherent photoproduction mechanism of J/ψ in hadronic collisions, more precise experimental measurements and more advanced models are required. The excess production from J/ψ may provide a novel probe for QGP; this requires further investigation.

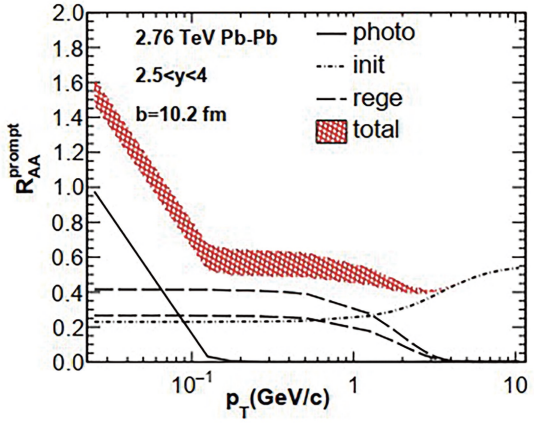


Fig. 13. Charmonium prompt nuclear modification factor as a function of transverse momentum for impact parameter b = 10.2 fm in the forward rapidity $2.5 < y < 4$ in LHC 2.76 TeV Pb + Pb collisions. Figure taken from Ref. [23].

3 Dileptons from coherent photon–photon interactions in hadronic heavy-ion collisions

Dileptons can be produced via the coherent photon–photon interaction $\gamma+\gamma \to e^+ + e^-$ or $\gamma+\gamma \to \mu^+ + \mu^-$ in ultra-peripheral heavy-ion collisions. As demonstrated in Section 2, coherent photon–nucleus interactions should occur in hadronic heavy-ion collisions. A similar process, coherent photon–photon interaction, should also be expected in hadronic heavy-ion collisions.

3.1 Measurements of the STAR Collaboration

The STAR Collaboration reported measurements of e^+e^- pair production in the mass region $0.4 < M_{ee} < 2.6$ GeV/c^2 at extremely low transverse momentum ($p_T < 0.15$ GeV/c) using the minimum-bias events collected during 2010 and 2012 in peripheral Au + Au and U + U collisions[14].

Fig. 14a shows the centrality dependence of the e^+e^- invariant mass spectra within the STAR acceptance for pair $p_T <$ 0.15 GeV/c, and Fig. 14b shows the enhancement factors, which are the ratios of the data over the hadronic cocktail as a function of the invariant mass. The enhancement factor of most peripheral collisions (60%–80%) is significant, though it becomes increasingly less from peripheral to semiperipheral (40%–60%) and semicentral (10%–40%) collisions[14]. In the low invariant mass region, the enhancement factors first decrease with the invariant mass, then increase above M_ϕ, and finally reach a maximum value around $M_{J/\psi}$.

Considering the different behaviors of the enhancement factor in different invariant mass regions, the mass can be divided into three mass bins (0.4–0.76, 0.76–1.2, and 1.2–2.6 GeV/c^2). Fig. 15 shows the transverse momentum distributions of the e^+e^- pairs for different mass bins in the 60%–80%

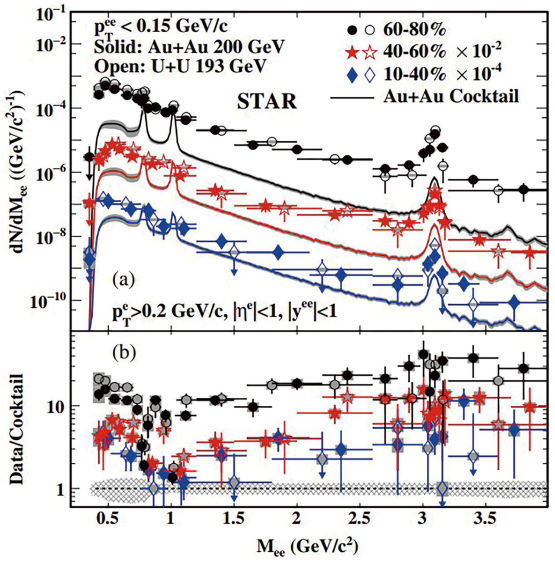


Fig. 14. (a) Centrality dependence of e^+e^- invariant mass spectra within the STAR acceptance from Au +Au and U + U collisions for pair $p_T <$ 0.15 GeV/c. (b) Corresponding ratios of data over cocktail. Figure taken from Ref. [14].

DOI: 10.52396/JUSTC-2021-0210
JUSTC, **2022**, 52(6): 3

Au + Au and U + U collisions. As shown in the figure, the contributions of the hadronic cocktail are consistent with the measurements for p_T > 0.15 GeV/c; however, the observed excess of the positron–electron pair production is found to be concentrated at very low transverse momentum (p_T < 0.15 GeV/c) in all three mass regions[14].

To study the production mechanism of the enhancement, the STAR Collaboration investigated the centrality dependence of the integrated excess yields in Au + Au and U + U collisions. Fig. 16 shows the excess yield spectra (data-cocktail) as a function of $N_{\rm part}$ after subtracting the hadronic cocktail contributions in different invariant mass bins. As shown in the figure, compared to the contribution of the hadronic cocktail, the excess yields show a much weaker dependence on collision centrality; this indicates that the hadronic cocktail alone is unlikely to be the source of the enhancement.

Fig. 17 shows the p_T^2 (≈–t, the squared four-momentum transfer) distributions of the excess yields in 60%–80% Au + Au and U + U collisions within the STAR acceptance: Panels Figs. 17a–17c show the results for three different mass bins. The solid and dotted lines are exponential fits to the data for the Au + Au and U + U collisions, respectively. Furthermore, the dot-dashed and dot-dot-dashed lines indicate the results of the two models [18,40] for the photon–photon process within the STAR acceptance in 60%–80% Au + Au and U + U collisions. The calculations from Ref. [40] are lower than the data points at high p_T^2 but exceed those at low p_T^2; meanwhile, the result from STARlight is lower than that from Ref. [40], though their shapes are similar.

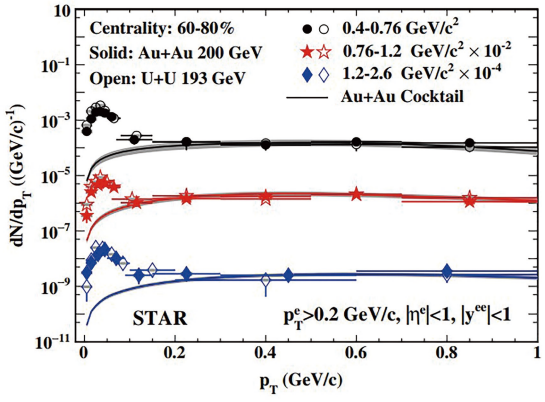


Fig. 15. e^+e^- pair p_T distributions within the STAR acceptance for different mass regions in 60%–80% Au + Au and U + U collisions with respect to the cocktail. Figure taken from Ref. [14].

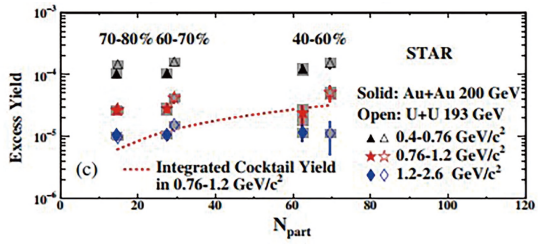


Fig. 16. Centrality dependence of integrated excess yields in the mass regions 0.4–0.76，0.76–1.2，1.2–2.6 GeV/c^2 in Au + Au and U + U collisions. The centrality dependence of the hadronic cocktail yields in the mass region 0.76–1.2 GeV/c^2 is also shown for comparison. Figure taken from Ref. [14].

Fig. 17d shows the invariant mass dependence of the p_T broadening $\sqrt{< p_T^2 >}$ from both the data and photon–photon model. The $\sqrt{< p_T^2 >}$ increases slightly with the invariant mass, and the $\sqrt{< p_T^2 >}$ from Au + Au collisions exceeds that from the U + U collisions. In Au + Au collisions, the values of $\sqrt{< p_T^2 >}$ extracted from the data are ~6.1σ, 3.3σ, and 1.8σ[40] above the model calculation results in the 0.4–0.76, 0.76–1.2, and 1.2–2.6 GeV/c^2 mass regions, respectively, suggesting another source of transverse momentum broadening in peripheral collisions. The blue dashed lines in Figs. 17a–17c show the corresponding p_T^2 distributions for e^+e^- pairs from the model [40] traversing 1 fm through a constant magnetic field of 10^{14} T perpendicular to the beam line ($eBL \approx 30$ MeV/c)[41,42]. The corresponding p_T^2 distributions can qualitatively describe the data expected at low p_T^2, and the $\sqrt{< p_T^2 >}$ increases by ~30 MeV/c, as shown in Fig. 17d; this suggests the presence of high magnetic fields in QGP[41–43].

3.2 Measurements of the ATLAS Collaboration

The ATLAS Collaboration recently reported measurements of the $\gamma\gamma \to \mu^+\mu^-$ process in $\sqrt{s_{\rm NN}}$ = 5.02 TeV Pb + Pb collisions at the LHC[15], where the integrated luminosity is 0.49 nb^{-1}. The data were recorded with the ATLAS detector using its inner detector, calorimeter, trigger, muon spectrometer, and data acquisition systems[44]. The muon pairs produced by the photon–photon interactions are distinguishable from those generated by other mechanisms through their angle and momentum correlations, which are further quantified using the acoplanarity parameter α and asymmetry parameter A, defined as respectively, where $\phi^{\pm}$ denotes the azimuth angles and $p_T^{\pm}$ indicates the transverse momenta of the muon pairs.

$$\alpha \equiv 1 - \frac{|\phi^+ - \phi^-|}{\pi} \tag{4}$$

$$A \equiv \left|\frac{p_T^+ - p_T^-}{p_T^+ + p_T^-}\right| \tag{5}$$

All oppositely charged muon pairs that met the trigger and event selection requirements were considered for analysis. The muons were identified by matching tracks in the inner detector to tracks in the muon spectrometer; meanwhile, each muon is required to have a transverse momentum p_T > 4 GeV/c and pseudo-rapidity $|\eta|$ < 2.4[45,46]. Owing to the low transverse momentum of the γγ system, the distributions of parameters α and A for the muon pairs produced by the photon–photon process peaked near zero. The α and A distributions include significant background from the decay of heavy-flavor hadrons[15]. These hadrons often decay after traveling a significant distance from the interaction point; thus, the background distributions have long tails and can be extracted from the data by stipulating that A > 0.15 and α > 0.02. To suppress the contribution from the decay of hadrons and Z bosons, the invariant mass requirement of muon pairs 4 GeV/c^2 < $m_{\mu^+\mu^-}$ < 45 GeV/c^2 is applied. The α and A distributions can be obtained from the data by selecting the other variables. A < 0.06 is required to obtain the α distribution, and the A distribution is obtained by requiring that α > 0.015.

DOI: 10.52396/JUSTC-2021-0210
JUSTC, **2022**, 52(6): 3

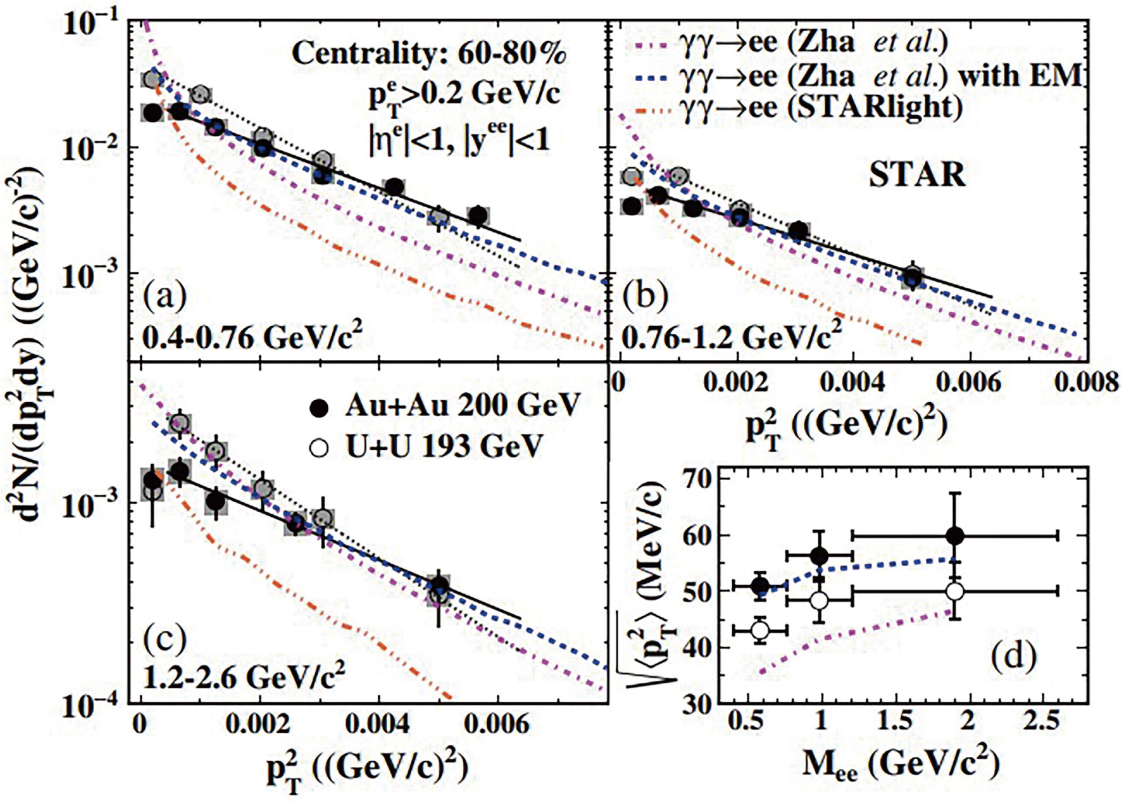


Fig. 17. (a)–(c) Distributions of excess yields within the STAR acceptance for the different mass regions in 60%–80% Au + Au and U + U collisions. (d) Corresponding $\sqrt{< p_T^2 >}$ of excess yields. Figure taken from Ref. [14].

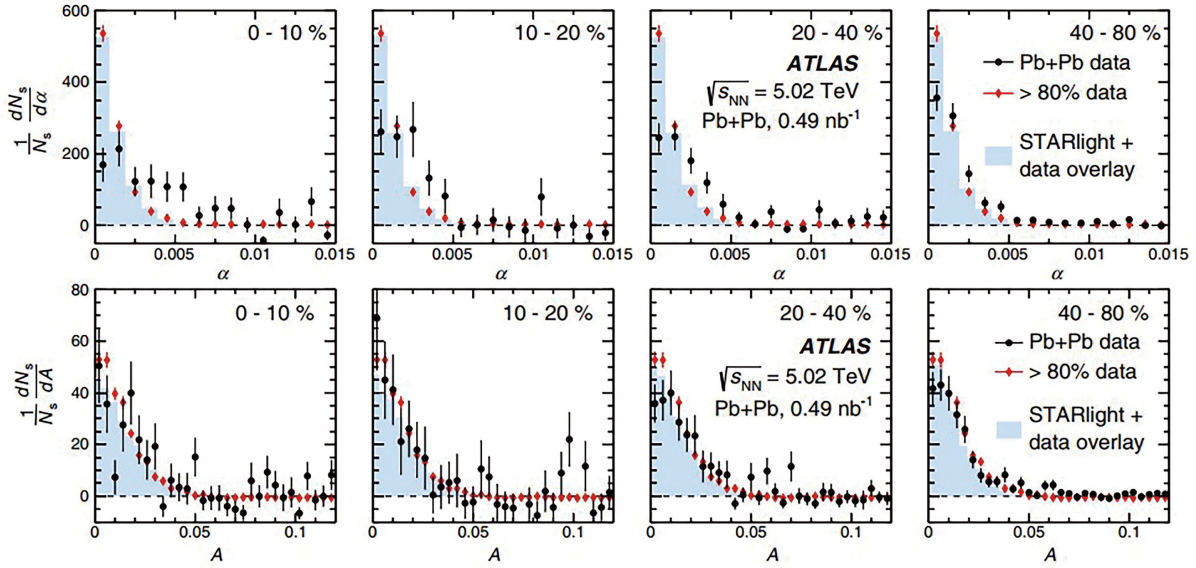


Fig. 18. Background-subtracted distributions for α (upper row) and A (lower row) in Pb + Pb collisions at $\sqrt{s_{NN}}$ = 5.02 TeV for different centrality classes. Each distribution is normalized to unity over its measured range. Figure taken from Ref. [15].

Fig. 18 shows the background-subtracted α distributions $(1/N_s)\mathrm{d}N_s/\mathrm{d}\alpha$ and A distributions $(1/N_s)\mathrm{d}N_s/\mathrm{d}A$, as measured in different centrality classes; the distribution with centrality > 80% and those generated by STARlight[19] and overlaid on the data (Monte Carlo simulation) are also plotted in the figure for comparison, where the > 80% interval includes the 80%–100% centrality class and ultra-peripheral collisions. Compared to the > 80% interval, a clear centrality-dependent broadening in the α distributions can be seen; no such effect is observed in the A distributions; this can be attributed to the momentum resolution of the ATLAS inner detector. The α distributions from the Monte Carlo simulation show almost no dependence on centrality, suggesting that the broadening of the data is much larger than that expected from the detect-

DOI: 10.52396/JUSTC-2021-0210
JUSTC, **2022**, 52(6): 3

or effects.

To further study the observed broadening in the α distributions, these distributions (background not subtracted) were fitted to a Gaussian function and the normalized background distribution. The solid lines represent the fit functions shown in Fig. 19, and the values of the width σ increase by a factor of two from the most peripheral bin to the most central one. Assume that the broadening of the α distributions results from a physical process that transfers an extremely small amount of transverse momentum, $\left|\overrightarrow{k_T}\right| \ll p_T^{\pm}$; then, the variance of the α distribution can be estimated as[15]

$$< \alpha^2 >= < \alpha^2 >_0 + \frac{1}{\pi^2} \frac{< \overrightarrow{k_T^2} >}{< p_{T\text{avg}}^2 >} \tag{6}$$

where $p_{T\text{avg}}$ is the mean of p_T^+ and p_T^-, and $< \alpha^2 >_0$ is the intrinsic mean square of α resulting from both the generation process itself and the angular resolution in the muon measurement. Taking $< \alpha^2 >_0$ to be the σ^2 from the Gaussian fit in the > 80% interval and taking $< \alpha^2 >$ to be the σ^2 from the Gaussian fit in each < 80% centrality class, the root mean square of $|\overrightarrow{k_T}|$, k_T^{rms}, can be approximated in that centrality class using the measured value of the root mean square of $p_{T\text{avg}}$, using Eq. (6). Fig. 20 shows the k_T^{rms} values as a function of $<N_{\text{part}}>$, which denotes the mean value of the participant nucleons in each centrality class and can be obtained from Glauber model analysis[24]. For the 0–10% centrality class, this procedure gives k_T^{rms} = 66 MeV ± 10 MeV.

The above fitting process provides a direct relationship between the widths of the α distributions and k_T^{rms}; however, it does not fully consider the influence of the shape of the $p_{T\text{avg}}$ distribution. Therefore, the Gaussian function in the fitting procedure was replaced by the convolution of the measured $p_{T\text{avg}}$ distribution and a Gaussian function. The results of the new fits are shown in Fig. 19, and the corresponding k_T^{rms} values calculated using Eq. (6) are shown in Fig. 20. In the 0–10% centrality class, k_T^{rms}= 70 ± 10 MeV. As shown in Fig. 20, the results of the two methods are consistent within their uncertainties, and the extracted k_T^{rms} is observed to increase with $<N_{\text{part}}>$. The k_T^{rms} values provide an estimate of the transverse momentum transfer associated with the absence of a physical mechanism in heavy-ion collisions.

3.3 Phenomenological model calculation

According to the equivalent photon approximation, the photon–photon interaction can be factorized into semiclassical and quantum parts: the former describes the photon distribution from the colliding ions and the latter describes the interaction between the two emitted photons [8]. In hadronic heavy-ion collisions, violent hadronic interactions occurring in the overlap region may result in destruction of the coherent action. The product of this process is the dilepton, which is not subject to strong interactions; therefore, in peripheral collisions, the destruction effect should be small, and the possible disruption can be neglected. However, for central collisions, the disruptive effect should be carefully considered in future studies.

The yields of coherent photon–photon interactions in relativistic heavy-ion collisions were calculated without considering the lepton pairs produced in the overlap region[40] ; this reduced the cross-section by ~20%. The disruptive effect of the hadronic interactions in the overlap region was neglected in the calculation. Fig. 21 shows the differential pair mass spectra of the electron and muon pairs produced by coherent photon–photon interactions in $\sqrt{s_{\text{NN}}}$ = 200 GeV Au + Au collisions and $\sqrt{s_{\text{NN}}}$ = 2.76 TeV Pb + Pb collisions for different centrality classes. The mass spectra for both electron and muon pairs show little dependence on centrality. They are very close in the high-mass region; however, the production rate of the muon pair is slightly lower than that of the electron pair in the lower-mass region.

In addition to coherent photon–photon interactions, dileptons can also be produced from the hadronic cocktail, in-medium ρ mass spectrum, and QGP thermal radiation. QGP thermal radiation refers to dileptons radiated from the interior of the dense medium throughout the lifetime of the fireball. To further compare the contributions of different sources, Fig. 22 shows the mass spectra of electron pairs produced via different production mechanisms in $\sqrt{s_{\text{NN}}}$ = 200 GeV Au + Au collisions for different centrality classes. For central collisions (0–10%), the hadronic contribution is dominant in the low mass region (0.4–2.0 GeV/c^2), and it approaches the contribution of photon–photon interactions at higher mass regions. They are comparable for semi-central collisions (10%–40%), and coherent photoproduction dominates for peripheral collisions (40%–80%). These results can reasonably describe the enhancement observed by the STAR Collaboration[14], indicating the existence of coherent photon–photon interactions in hadronic heavy-ion collisions.

Compared with coherent photonuclear interactions, the production rate of coherent photon–photon interactions is proportional to Z^4, depending on the equivalent photon approximation; this means that a more significant difference should be present between isobaric and Au + Au collisions. Fig. 23

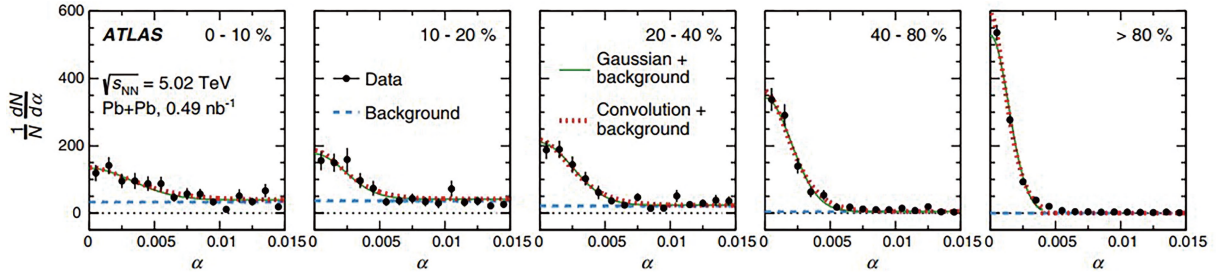


Fig. 19. Results of fits to the muon pair α distributions using the sum of Gaussian and background functions. A standard Gaussian function is shown as a solid curve whilst the dotted curve shows a Gaussian function in α convolved with the measured $p_{T\text{avg}}$ distribution. Figure taken from Ref. [15].

DOI: 10.52396/JUSTC-2021-0210
JUSTC, **2022**, 52(6): 3

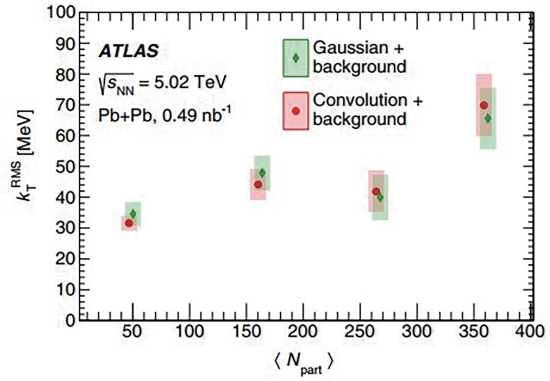


Fig. 20. k_T^{rms} values obtained from the fits shown in Fig. 19, expressed as a function of $<N_{part}>$. Figure taken from Ref. [15].

shows the invariant mass spectrum of the electron–positron pair from coherent photon–photon interaction and the decay of coherently photoproduced J/ψ in $\sqrt{s_{NN}}$ = 200 GeV Au + Au collisions for the 60%–80% centrality class as well as Ru + Ru and Zr + Zr collisions for the 47%–75% centrality class. Centrality in isobaric collisions is selected to ensure that the hadronic background contribution is consistent with that in Au + Au collisions. The in-medium ρ mass spectrum, QGP thermal radiation, and STAR measurements are also plotted in the figure for comparison. The relative yield ratios from the coherent photon–photon process for Au + Au, Ru + Ru, and Zr + Zr collisions are 7.9 ： 1.5 ： 1.0 [30]. Such large differences make it feasible to test the photoproduction mechanism during isobaric collisions.

The STAR Collaboration found a significant p_T broadening effect, by measuring the p_T^2 distribution of dileptons in hadronic Au + Au and U + U collisions with respect to EPA calculations[14] (Fig. 17). The ATLAS Collaboration also observed this broadening via the acoplanarity parameter α of muon pairs in hadronic Pb + Pb collisions [15] (Fig. 18). The broadening effect can be described by introducing the effect of the magnetic field in the QGP, or alternatively by the electromagnetic scattering of dileptons in the hot medium. Ref. [47] calculated the p_T^2 distribution and α distribution of dileptons produced by photon–photon interactions in heavy-ion collisions using the external classical field approach[48] and the generalized equivalent photon approximation (gEPA1). The results from the gEPA1 method significantly differed from the experimental data points; hence, an additional phase term is used for the empirical solution (i.e., the gEPA2 method).

Fig. 24 shows the p_T^2 distributions of the positron–electron pairs in 60%–80% Au + Au collisions at $\sqrt{s_{NN}}$ = 200 GeV within the STAR acceptance for the mass regions 0.4–0.76, 0.76–1.2, and 1.2–2.6 GeV/c^2; the transverse momentum is

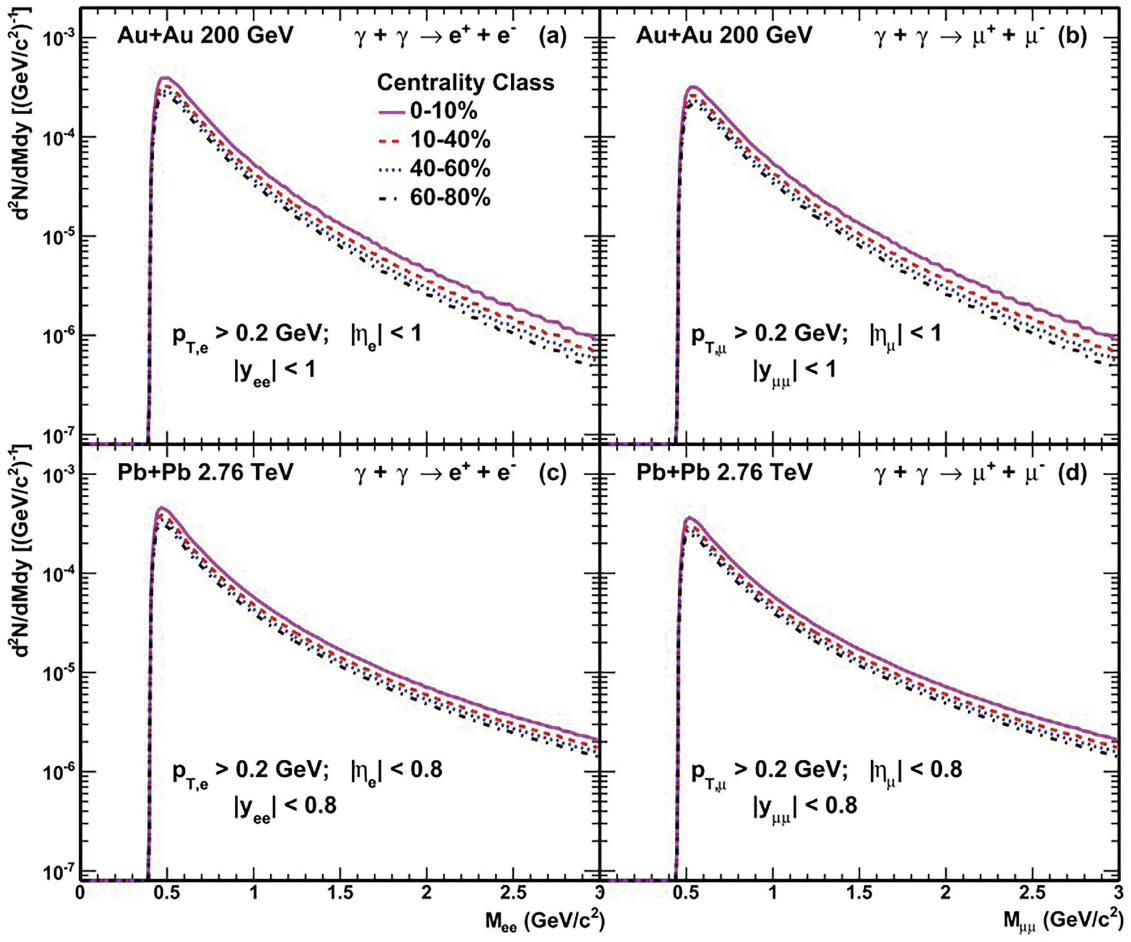


Fig. 21. Differential pair mass spectrum $d^2N/(dMdy)$ for (a) electron and (b) muon pairs with gold beams at RHIC and for (c) electron and (d) muon pairs with lead beams at LHC. The different curves in the figure indicate the results for different centrality classes. Figure taken from Ref. [40].

DOI: 10.52396/JUSTC-2021-0210
JUSTC, **2022**, 52(6): 3

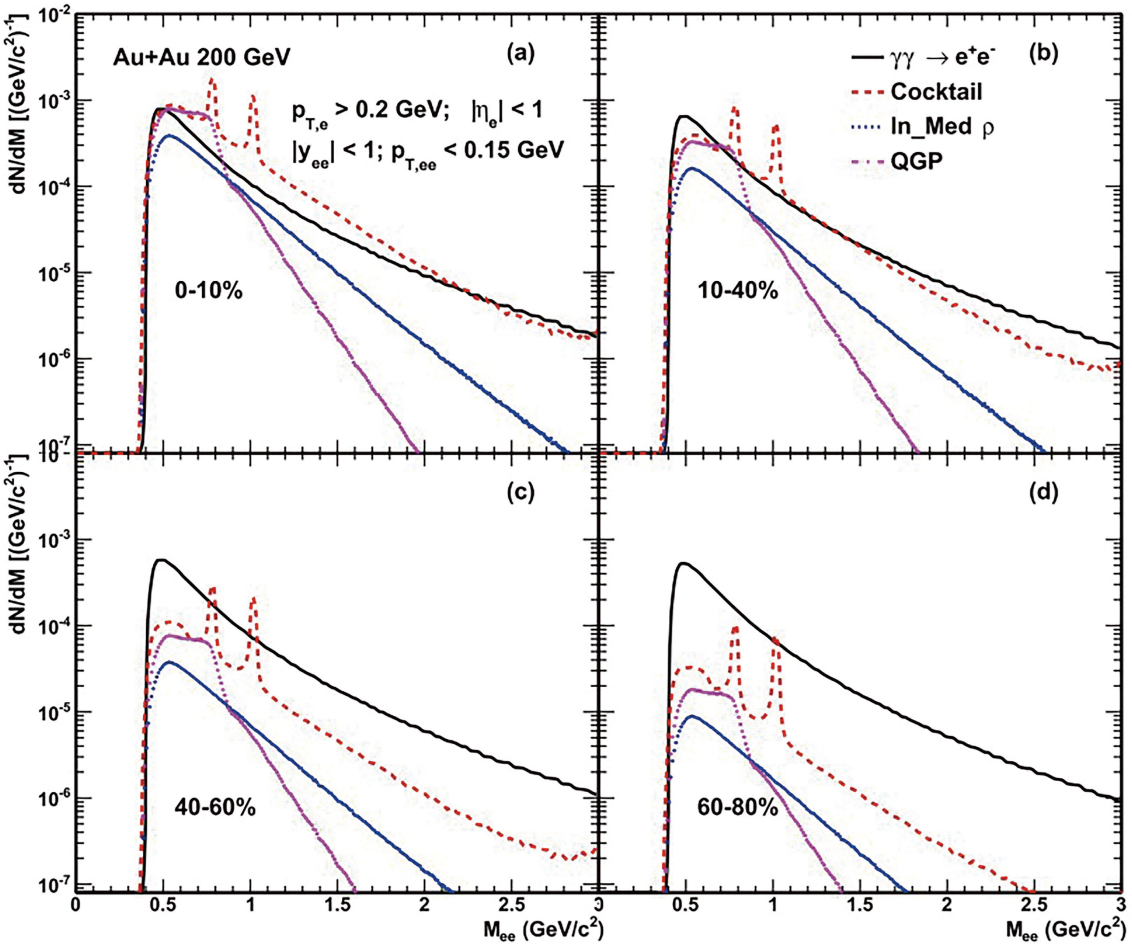


Fig. 22. Mass spectrum of electron pairs for different centrality classes. The mass distributions are compared to hadronic cocktail simulations without the ρ contribution in-medium ρ mass spectrum and QGP thermal radiation. Figure taken from Ref. [40].

denoted as $p_{\perp}$. The measurements from the STAR Collaboration[14] and calculations from gEPA1, gEPA2, quantum electrodynamics (QED)[49, 50], and STARlight[19] are also plotted in the figure for comparison. Both the QED and gEPA2 results describe the measurements well, and the QED calculation has a systematically lower $\sqrt{< p_T^2 >}$ than the STAR data and gEPA2 results.

Fig. 25 shows the transverse momentum broadening $\sqrt{< p_T^2 >}$ of electron–positron pairs as a function of the impact parameter for different mass regions in $\sqrt{s_{\rm NN}}$ = 200 GeV Au + Au collisions. The invariant mass dependence of the broadening can be seen in the figure: the higher the invariant mass, the more significant the broadening. The broadening from the QED calculation increased with the decreasing impact parameter and then reached its maximum value; the QED calculations were systematically lower than the STAR measurements. This may be attributable to the final-state broadening effect, which requires further research and exploration in the future.

Ref. [47] also calculated the α distributions from the generalized EPA and QED approach in $\sqrt{s_{NN}}$ = 5.02 TeV Pb + Pb collisions for different centrality classes, as shown in Fig. 26. The gEPA2 and QED calculations can accurately describe the measurements from ATLAS[15] (within uncertainties). The results of the gEPA1 and gEPA2 methods are consistent in UPCs and peripheral collisions; however, in central collisions, the results of gEPA1 differ substantially from the measurements and other model calculations. The above calculations indicate that the transverse momentum broadening and acoplanarity broadening are mainly attributable to the initial electromagnetic field strength, which is significantly affected by the impact parameter. An additional small broadening may arise from the final-state interaction, which requires validation

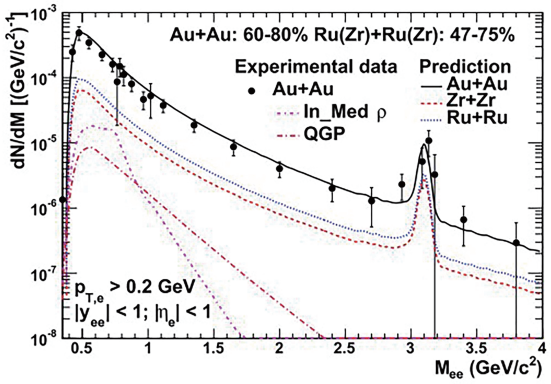


Fig. 23. Invariant mass spectrum of e^+e^- pair from coherent photon–photon interaction and decay of coherently produced J/ψ in Au + Au collisions for 60%–80% centrality class as well as Ru + Ru and Zr + Zr collisions for 47%–75% centrality class. Figure taken from Ref. [30].

DOI: 10.52396/JUSTC-2021-0210
JUSTC, **2022**, 52(6): 3

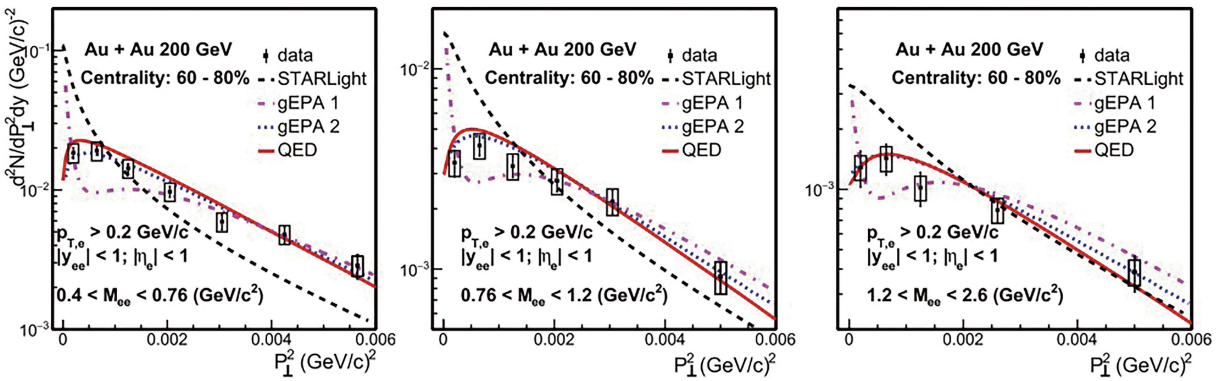


Fig. 24. p_T^2 distributions of electron–positron pair production within the STAR acceptance for three different mass regions in 60%–80% Au + Au collisions at $\sqrt{s_{NN}}$ = 200 GeV. Figure taken from Ref. [47].

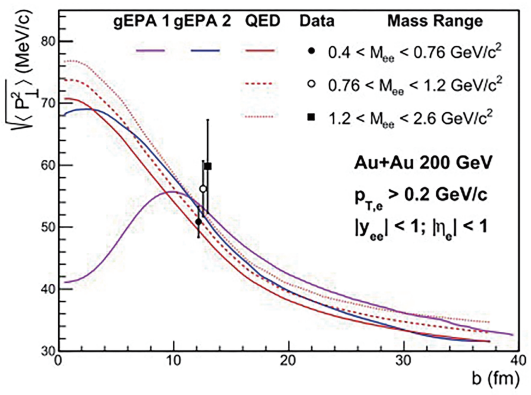


Fig. 25. $\sqrt{< p_T^2 >}$ of electron–positron pairs within the STAR acceptance as a function of the impact parameter b for different mass regions in Au + Au collisions at $\sqrt{s_{NN}}$ = 200 GeV. Figure taken from Ref. [47].

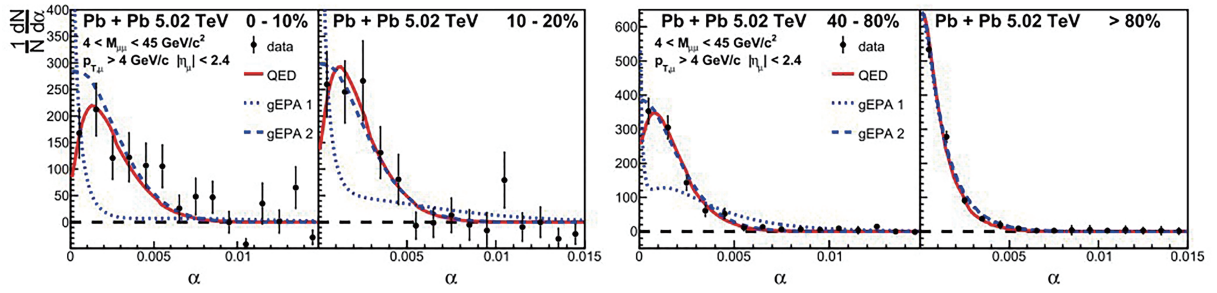


Fig. 26. Distributions of the broadening variable α obtained from the gEPA1, gEPA2, and QED approaches for muon pairs in Pb + Pb collisions at $\sqrt{s_{NN}}$ = 5.02 TeV in different centrality classes. Figure taken from Ref. [47].

4 Discussion and prospects

This review summarizes the recent experimental and theoretical progress in coherent photoproduction in hadronic heavy-ion collisions. The STAR, ALICE, and ATLAS Collaborations have observed significant enhancements in J/ψ and dilepton production at very low transverse momentum in peripheral collisions. According to the calculations of the phenomenological model, the excesses may result from coherent photon–nucleus and photon–photon interactions, respectively. Violent hadronic interactions that occur in the overlap region may lead to the destruction of coherent action, which is absent in ultra-peripheral collisions. J/ψ and dileptons, originating from the coherent photoproduction process in relativistic heavy-ion collisions, may serve as new novel probes to study the evolution of QGP and determine the electromagnetic properties of QGP.

3.4 Summary

The STAR and ATLAS Collaborations have recently observed significant enhancements in the dilepton yields at very low transverse momentum in hadronic heavy-ion collisions. This excess may result from coherent photon–photon interactions, and phenomenological model calculations support this conclusion. Different phenomenological models provide different predictions of transverse momentum distributions; this calls for more precise and differentiated experimental measurements. This is crucially important for further probing the electromagnetic properties of QGP using the transverse momentum distribution of the dilepton. Furthermore, the destruction of coherent action from violent hadronic interactions in the overlap region was neglected in the models, which should be considered in future work.

Acknowledgements

This work was supported by the National Natural Science Foundation of China (11775213, 12005220) and the USTC Research Funds of the Double First-Class Initiative (YD2360002001).

Conflict of interest

The authors declare that they have no conflicts of interest.

DOI: 10.52396/JUSTC-2021-0210
JUSTC, **2022**, 52(6): 3

Biographies

Jiaxuan Luo is currently a graduate student under the tutelage of Assoc. Prof. Wangmei Zha at the University of Science and Technology of China. His research interests focus on particle physics and nuclear physics.

Wangmei Zha is an Associate Professor at the University of Science and Technology of China (USTC). He received the Ph.D. degree from the USTC in 2014. From then to 2016, he conducted postdoctoral research at the USTC. He joined the USTC in 2016. He is primarily engaged in the data analysis of relativistic heavy-ion collisions and the construction, maintenance, calibration, and software development of the muon detector. His research results have been published in *Physical Review Letter, Physical Letter B, Journal of High Energy Physics, Chinese Physics C, Physical Review D,* and other academic journals.

References

[1] Braun-Munzinger P, Stachel J. The quest for the quark-gluon plasma. *Nature,* **2007**, *448*: 302–309.

[2] Matsui T, Satz H. J/ψ suppression by quark-gluon plasma formation. *Physics Letters B,* **1986**, *178* (4): 416–422.

[3] Yan L, Zhuang P F, Xu N. J/ψ production in quark-gluon plasma. *Physical Review Letters,* **2006**, *97*: 232301.

[4] Ferreiro E G, Fleuret F, Lansberg J P, et al. Cold nuclear matter effects on J/ψ production: Intrinsic and extrinsic transverse momentum effects. *Physics Letters B,* **2009**, *680* (1): 50–55.

[5] Adamczyk L, Adkins J K, Agakishiev G, et al. (STAR Collaboration). Energy dependence of J/ψ production in Au+Au collisions at $\sqrt{s_{NN}}$=39, 62.4 and 200 GeV. *Physics Letters B,* **2017**, *771*: 13–20.

[6] van Hees H, Rapp R. Dilepton radiation at the CERN super-proton synchrotron. *Nuclear Physics A,* **2008**, *806*: 339–387.

[7] Rapp R. Dilepton spectroscopy of QCD matter at collider energies. *Advances in High Energy Physics,* **2013**, *2013*: 148253.

[8] Krauss F, Greiner M, Soff G. Photon and gluon induced processes in relativistic heavy-ion collisions. *Progress in Particle and Nuclear Physics,* **1997**, *39*: 503–564.

[9] Fermi E. Über die Theorie des Stoßes zwischen Atomen und elektrisch geladenen Teilchen. *Zeitschrift für Physik,* **1924**, *29*: 315–327.

[10] Weizsäcker C F V. Ausstrahlung bei Stößen sehr schneller Elektronen. *Zeitschrift für Physik,* **1934**, *88*: 612–625.

[11] Adler C, Ahammed Z, Allgower C, et al. (STAR Collaboration). Coherent ρ^0 production in ultraperipheral heavy-ion collisions. *Physical Review Letters,* **2002**, *89*: 272302.

[12] Adam J, et al. (ALICE Collaboration). Measurement of an excess in the yield of J/ψ at very low p_T in Pb–Pb collisions at $\sqrt{s_{NN}}$=2.76 TeV. *Physical Review Letters,* **2016**, *116*: 222301.

[13] Adam J, Adamczyk L, Adams J R, et al. (STAR Collaboration). Observation of excess J/ψ yield at very low transverse momenta in Au+Au collisions at $\sqrt{s_{NN}}$=200 GeV and U+U collisions at $\sqrt{s_{NN}}$=193 GeV. *Physical Review Letters,* **2019**, *123*: 132302.

[14] Adam J, Adamczyk L, Adams J R, et al. (STAR Collaboration). Low-p_T e^+e^- pair production in Au+Au collisions at $\sqrt{s_{NN}}$=200 GeV and U+U collisions at $\sqrt{s_{NN}}$=193 GeV at STAR. *Physical Review Letters,* **2018**, *121*: 132301.

[15] Aaboud M, Aad G, Abbott B, et al. (ATLAS Collaboration). Observation of centrality-dependent acoplanarity for muon pairs produced via two-photon scattering in Pb+Pb collisions at $\sqrt{s_{NN}}$=5.02 TeV with the ATLAS detector. *Physical Review Letters,* **2018**, *121*: 212301.

[16] Guzey V, Zhalov M. Exclusive J/ψ production in ultraperipheral collisions at the LHC: Constraints on the gluon distributions in the proton and nuclei. *Journal of High Energy Physics,* **2013**, *2013*: 207.

[17] The ALICE Collaboration, Aamodt K, Quintana A A, et al. (ALICE Collaboration). The ALICE experiment at the CERN LHC. *Journal of Instrumentation,* **2008**, *3*: S08002.

[18] Abelev B, Abramyan A, Adam J, et al. (ALICE Collaboration). Performance of the ALICE experiment at the CERN LHC. *International Journal of Modern Physics A,* **2014**, *29*: 1430044.

[19] Klein S R, Nystrand J, Seger J, et al. STARlight: A Monte Carlo simulation program for ultra-peripheral collisions of relativistic ions. *Computer Physics Communications,* **2017**, *212*: 258–268.

[20] Liu Y P, Qu Z, Xu N, et al. J/ψ transverse momentum distribution in high energy nuclear collisions. *Physics Letters B,* **2009**, *678* (1): 72–76.

[21] Zhao X B, Rapp R. Charmonium in medium: From correlators to experiment. *Physical Review C,* **2010**, *82*: 064905.

[22] Abelev B, et al. (ALICE Collaboration). Coherent J/ψ photoproduction in ultra-peripheral Pb–Pb collisions at $\sqrt{s_{NN}}$=2.76 TeV. *Physics Letters B,* **2013**, *718*: 1273–1283.

[23] Shi W, Zha W, Chen B Y. Charmonium coherent photoproduction and hadroproduction with effects of quark gluon plasma. *Physics Letters B,* **2018**, *777*: 399–405.

[24] Miller M L, Reygers K, Sanders S J, et al. Glauber modeling in high-energy nuclear collisions. *Annual Review of Nuclear and Particle Science,* **2007**, *57*: 205–243.

[25] Tanabashi M, et al. (Particle Data Group). Review of particle physics. *Physical Review D,* **2018**, *98*: 030001.

[26] Bertulani C A, Klein S R, Nystrand J. Physics of ultra-peripheral nuclear collisions. *Annual Review of Nuclear and Particle Science,* **2005**, *55*: 271–310.

[27] Zha W, Huang B C, Ma R R, et al. Systematic study of the experimental measurements on J/ψ cross sections and kinematic distributions in p+p collisions at different energies. *Physical Review C,* **2016**, *93*: 024919.

[28] Zha W M, Klein S R, Ma R, et al. Coherent J/ψ photoproduction in hadronic heavy-ion collisions. *Physical Review C,* **2018**, *97*: 044910.

[29] Bauer T H, Spital R D, Yennie D R, et al. The hadronic properties of the photon in high-energy interactions. *Review of Modern Physics,* **1978**, *50*: 261.

[30] Zha W, Ruan L, Tang Z, et al. Coherent photo-produced J/ψ and dielectron yields in isobaric collisions. *Physics Letters B,* **2019**, *789*: 238–242.

[31] Jönsson C. Elektroneninterferenzen an mehreren künstlich hergestellten Feinspalten. *Zeitschrift für Physik,* **1961**, *161(4)*: 454–474.

[32] Zeilinger A, Gähler R, C. G. Shull, et al. Single- and double-slit diffraction of neutrons. *Review of Modern Physics,* **1988**, *60*: 1067.

[33] Carnal O, Mlynek J. Young's double-slit experiment with atoms: A simple atom interferometer. *Physical Review Letters,* **1991**, *66*: 2689.

[34] Arndt M, Nairz O, Vos-Andreae J, et al. Wave–particle duality of C_{60} molecules. *Nature,* **1999**, *401*: 680–682.

[35] Hackermüller L, Uttenthaler S, Hornberger K, et al. Wave nature of biomolecules and fluorofullerenes. *Physical Review Letters,* **2003**, *91*: 090408.

[36] Zha W, Ruan L, Tang Z, et al. Double-slit experiment at Fermi scale: Coherent photoproduction in heavy-ion collisions. *Physical Review C,* **2019**, *99*: 061901.

[37] Barrett R C, Jackson D F. Nuclear Sizes and Structure. Oxford, UK: Oxford University Press, **1977**.

[38] Matsui T, Satz H. J/ψ suppression by quark-gluon plasma formation. *Physics Letters B,* **1986**, *178* (4): 416–422.

[39] Chen B Y. Detailed rapidity dependence of J/ψ production at energies available at the Large Hadron Collider. *Physical Review C,* **2016**, *93*: 054905.

[40] Zha W, Ruan L, Tang Z, et al. Coherent lepton pair production in hadronic heavy ion collisions. *Physics Letters B,* **2018**, *781*: 182–186.

DOI: 10.52396/JUSTC-2021-0210
JUSTC, **2022**, 52(6): 3

[41] Inghirami G, Del Zanna L, Beraudo A, et al. Numerical magneto-hydrodynamics for relativistic nuclear collisions. *The European Physical Journal C,* **2016**, *76* (12): 659.
[42] Asakawa M, Majumder A, Muller B. Electric charge separation in strong transient magnetic fields. *Physical Review C,* **2010**, *81*: 064912.
[43] Kharzeev D E, Warringa H J. Chiral magnetic conductivity. *Physical Review D,* **2009**, *80*: 034028.
[44] The ATLAS Collaboration1, Aad G, Abat E, et al. (ATLAS Collaboration). The ATLAS experiment at the CERN Large Hadron Collider. *Journal of Instrumentation,* **2008**, *3*: S08003.
[45] ATLAS Collaboration, Aad G, Abbott B, et al. (ATLAS Collaboration). Measurement of the muon reconstruction performance of the ATLAS detector using 2011 and 2012 LHC proton-proton collision data. *The European Physical Journal C,* **2014**, *74*: 3130.
[46] ATLAS Collaboration, Aad G, Abbott B, et al. (ATLAS Collaboration). Muon reconstruction performance of the ATLAS detector in proton–proton collision data at $\sqrt{s}$=13 TeV. *The European Physical Journal C,* **2016**, *76*: 292.
[47] Zha W, Brandenburg J D, Tang Z, et al. Initial transverse-momentum broadening of Breit-Wheeler process in relativistic heavy-ion collisions. *Physics Letters B,* **2020**, *800*: 135089.
[48] Vidović M, Greiner M, Best C, et al. Impact-parameter dependence of the electromagnetic particle production in ultrarelativistic heavy-ion collisions. *Physical Review C,* **1993**, *47*: 2308.
[49] Hencken K, Trautmann D, Baur G. Impact-parameter dependence of the total probability for electromagnetic electron-positron pair production in relativistic heavy-ion collisions. *Physical Review A,* **1995**, *51*: 1874.
[50] Alscher A, Hencken K, Trautmann D, et al. Multiple electromagnetic electron-positron pair production in relativistic heavy-ion collisions. *Physical Review A,* **1997**, *55*: 396.
[51] Adams J, Aggarwal M M, Ahammed Z, et al. (STAR Collaboration). Production of e^+e^- pairs accompanied by nuclear dissociation in ultraperipheral heavy-ion collisions. *Physical Review C,* **2004**, *70*: 031902.
[52] Abelev B, et al. (ALICE Collaboration). *J/ψ* suppression at forward rapidity in Pb-Pb collisions at $\sqrt{s_{NN}}$ = 2.76 TeV. *Physical Review Letters,* **2012**, *109*: 072301.
[53] Abelev B I, et al. (STAR Collaboration). ρ^0 photoproduction in ultraperipheral relativistic heavy ion collisions at $\sqrt{s_{NN}}$=200 GeV. *Physical Review C,* **2008**, *77*: 034910.
[54] PHENIX Collaboration, S.Afanasiev S, Aidalag C, et al. (PHENIX Collaboration). Photoproduction of *J/ψ* and of high mass e^+e^- in ultra-peripheral Au+Au collisions at $\sqrt{s_{NN}}$=200 GeV. *Physics Letters B,* **2009**, *679* (4): 321–329.
[55] The ALICE Collaboration, Abbas E, Abelev B, et al. (ALICE Collaboration). Charmonium and e^+e^- pair photoproduction at mid-rapidity in ultra-peripheral Pb–Pb collisions at $\sqrt{s_{NN}}$ =2.76 TeV. *The European Physical Journal C,* **2013**, *73*: 2617.
[56] Khachatryan V, Sirunyan A M, Tumasyan A, et al. (CMS Collaboration). Coherent *J/ψ* photoproduction in ultra-peripheral Pb-Pb collisions at $\sqrt{s_{NN}}$=2.76 TeV with the CMS experiment. *Physics Letters B,* **2017**, *772*: 489–511.
[57] Abelevbv B, Adamal J, Adamová D, et al. (ALICE Collaboration). Centrality, rapidity and transverse momentum dependence of *J/ψ* suppression in Pb-Pb collisions at $\sqrt{s_{NN}}$= 2.76 TeV. *Physics Letters B,* **2014**, *734*: 314–327.
[58] Klein S R. Two-photon production of dilepton pairs in peripheral heavy ion collisions. *Physical Review C,* **2018**, *97*: 054903.

DOI: 10.52396/JUSTC-2021-0210
JUSTC, **2022**, 52(6): 3